Geothermics 131 (2025) 103375

Contents lists available at ScienceDirect

Geothermics

journal homepage: www.elsevier.com/locate/geothermics

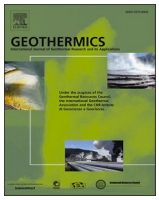

Influence of magma chamber on the formation of high-temperature geothermal resource in volcanic geothermal systems: A case study of the Changbai mountain region

Jialin Song [a,b], Nansheng Qiu [a,b,c,*], Qianqian Feng [a,c], Chuanqing Zhu [a,b], Yonghui Huang [a,b], Keyan Liao [a,b], Zhanwen Zhang [a,b], Yike Zhou [a,b]

[a] National Key Laboratory of Petroleum Resource and Engineering, China University of Petroleum, Beijing 102249, China
[b] College of Geosciences, China University of Petroleum, Beijing 102249, China
[c] College of Carbon Neutral Energy, China University of Petroleum, Beijing 102249, China

ARTICLE INFO

Keywords:
High-temperature geothermal resources
Magma chamber
Volcanic geothermal system
Changbai mountain
Surface heat flow
Geothermal power generation

ABSTRACT

Magma chambers significantly influence geothermal temperature distribution, particularly in forming high-temperature (>150 °C) geothermal resources. This study investigates the role of magma chambers in controlling geothermal temperature distribution, with a focus on the Changbai Mountain volcanic geothermal system, located within the Circum-Pacific Geothermal Belt. Despite extensive surface manifestations of medium-low temperature hot springs, the region lacks high-temperature geothermal features. By integrating drilling data, geophysical surveys, and geochemical analyses, a three-dimensional geological model was constructed, revealing an elliptical magma chamber (30 km east-west, 70 km north-south) as a significant heat source which influences an area of ~11,780 km^2, The surface heat flow value of Changbai Mountain region ranging from 70.1 to 130.8 mW/m^2 (average 83.8 mW/m^2), of which ~10.3 mW/m^2 is directly attributable to the magma chamber. The 150°C isotherm burial depth ranges from 2.35 to 4.43 km, with the shallowest depths distributed in the chamber's thermal influence zone. The geothermal resource potential of the 2-4 km carbonate reservoir is estimated at ~5.79×10^{20} J, corresponding to a power generation potential of ~6759.4 MWe, with an additional ~262.4 MWe contributed by the magma chamber. This study provides a reliable model and case reference for geothermal resource assessment in volcanic geothermal systems, offering quantitative data to support the exploitation of high-temperature geothermal resources in magma chamber-associated volcanic systems.

1. Introduction

China's high-temperature geothermal resources are primarily distributed in two geothermal belts: the Mediterranean-Himalayan Geothermal Belt and the Circum-Pacific Geothermal Belt (Wang, 2015; Wang et al., 2017; Pang et al., 2014). Surrounding the Circum-Pacific Geothermal Belt, the Changbai Mountain region is recognized for its significant geothermal resource potential, characterized by extensive hot spring manifestations and active volcanic activities. Located along the China-North Korea border within the Eurasian Plate, this area hosts China's largest Cenozoic active volcanic system and represents a well-developed volcanic geothermal system (Figure 1) (Wei et al., 2016; Wei et al., 2013). Since the Miocene, the Changbai Mountain volcano has experienced multiple eruptions, generating substantial volumes of volcanic pyroclastic and volcanic ash (Hakozaki et al., 2018). Evidence of these eruptions has been identified as far as the Kuril Trench, approximately 2000 kilometers away, demonstrating the significant scale and impact of these volcanic events (Horn and Schmincke, 2000; Nanayama et al., 2003). Up to the present day, the Changbai Mountain volcano continues to exhibit significant geological activity,characterized by frequent tectonic earthquakes (Ming et al., 2006;Wu et al., 2007; Xu et al., 2012), intense volcanic gas emissions (Gao et al., 2006), and the presence of a residual magma chamber at depth (Tang et al., 2001; Zhang et al., 2002; Chou et al., 2014; Guan et al., 2020; Ruan et al., 2020, Jiang et al., 2023). Volcanic geothermal systems globally exhibit significant high-temperature geothermal potential (Stelling et al., 2016; Chiodini et al., 2014). For example, the Sokoria Geothermal Field in Indonesia has a geothermal reservoir depth ranging from 600m to

* Corresponding author.
E-mail address: qiunsh@cup.edu.cn (N. Qiu).

https://doi.org/10.1016/j.geothermics.2025.103375
Received 21 March 2025; Received in revised form 9 April 2025; Accepted 1 May 2025
Available online 8 May 2025

1400m, with fluid temperatures between 220 °C and 260 °C, and a geothermal power generation capacity of 30 MWe (Sarmiento et. al, 2019). However, in the Changbai Mountain area, there is no high-temperature hydrothermal activity at the surface, with the highest temperature at the spring outlets reaching 82 °C, which is below the local boiling point (Yan, 2016). Therefore, the high-temperature geothermal resource potential of this volcanic geothermal system remains underexplored.

Contemporary volcanic activity serves as the most direct evidence for the presence of high-temperature ascending magma within the Earth's crust. The magma chamber remains in the crust represents an ideal heat source for the formation of high-temperature geothermal systems. Although surface manifestations of high-temperature hydrothermal systems are absent in the Changbai Mountain region, the intense volcanic activity suggests the possible existence of concealed high-temperature geothermal systems at depth (Zhang et al., 2024). The crustal magma chamber maintains significantly higher temperatures than the surrounding crust, providing additional thermal energy through prolonged thermal baking. By using geophysical methods, geochemical analyses, and numerical simulation forward modeling, previous studies have confirmed the existence of a shallow magma chamber beneath the Changbai Mountain region (Tang et al., 2001; Zhang et al., 2002; Chou et al., 2014; Guan et al., 2020; Ruan et al., 2020; Jiang et al., 2023). Through geological mapping, geological surveys, drill core sample observations, magnetotelluric profile interpretation, and seismic tomography data analysis, researchers have established a two-dimensional geological model centered on Changbai Mountain. This model simulates the temperature distribution along the profile and evaluates the influence of the magma chamber on thermal patterns, identifying favorable hydrothermal geothermal reservoirs at depths of 2-4 km and hot dry rock (HDR) geothermal reservoirs at depths of 4-7 km (Cheng et al., 2024). Despite extensive geological, geochemical, geophysical, and hydrological investigations conducted by previous researchers, the high-temperature geothermal resource potential of the Changbai Mountain region remains inadequately assessed. The relationship between the magma chamber and high-temperature geothermal resources in this area is still not fully understood. This study establishes a rock thermal property column for the Changbai Mountain region based on thermal conductivity measurements from 93 outcrop samples and heat production rate data from 42 outcrop samples, supplemented by previous thermophysical data. Integrating existing magnetotelluric and seismic data with other geological and geophysical information, we have developed a three-dimensional geological model of the region. Using numerical simulation methods, we have modeled the subsurface heat conduction processes in the Changbai Mountain area, validating the model's reliability by comparing simulation results with measured data from geothermal wells. Based on the simulation results, we analyze the temperature and surface heat flow distribution in the Changbai Mountain region. The study quantifies the geothermal reservoir resources and power generation potential, while evaluating the influence of the magma chamber on regional geothermal distribution patterns.

2. Geological settings and volcano evolution

The Changbai Mountain region is situated along the China-North Korea border at the leading edge of the Pacific Plate subduction zone. Its tectonic position lies at the northeastern margin of the North China Craton, within the active continental margin tectonic environment resulting from the interaction between the Eurasian and Pacific Plates. This region forms part of the Circum-West Pacific magmatic-tectonic belt. The formation of Changbai Mountain is closely related to the subduction of the Pacific Plate beneath the Eurasian Plate. Since the Cenozoic era, the Pacific Plate has undergone significant tectonic evolution: (1) 55-25 Ma: Shallow-angle subduction of the Pacific Plate; (2) 25-15 Ma: Trench retreat and slab rollback occurred; (3) Since 15 Ma:

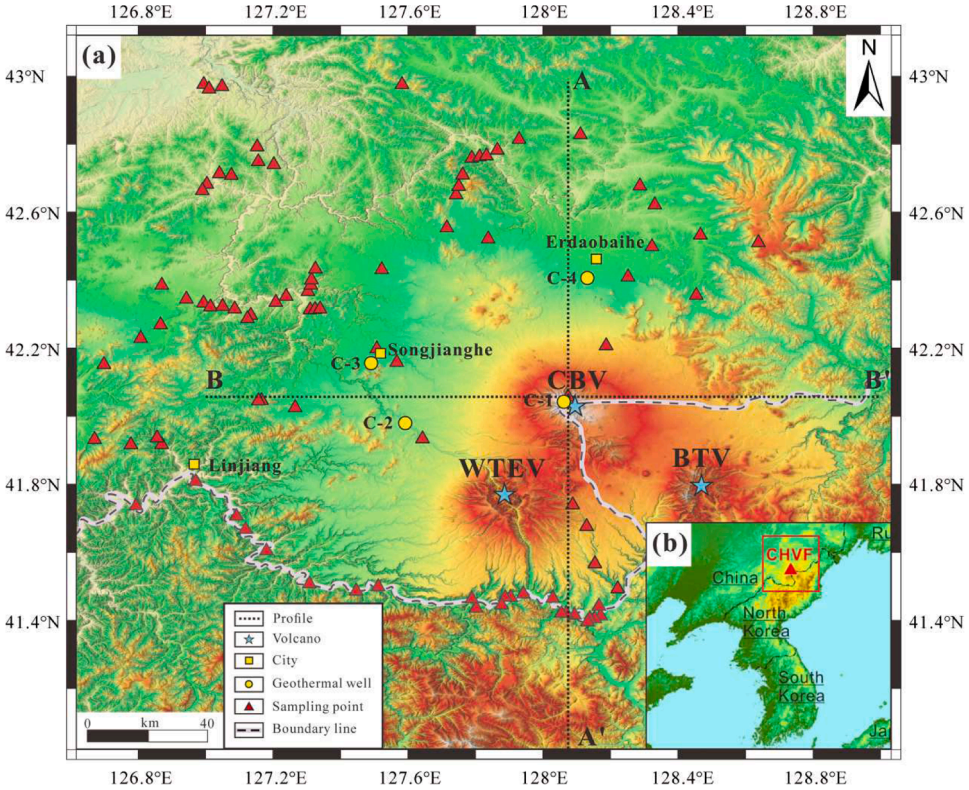

Figure 1. (a) Volcanic distribution and topographic map of the Changbai Mountain region (CBV: Changbai Volcano, WTEV: Wangtian'e Volcano, BTV: Baotaoshan Volcano. Elevation data sourced from SRTM database). (b) Location map of the Changbai Mountain region (CHVF: Changbai Volcanic Field, modified from Zhang et al., 2018).

The Pacific Plate has ultimately entered the mantle transition zone, reaching its base, leaving behind a stagnant, thickened, and flattened slab, over which a large mantle wedge has formed (Zhang et al., 2018).

The Changbai Mountain volcano, classified as an intraplate volcano, comprises an extensive lava plateau, numerous volcanic vents, and three primary eruptive centers: Tianchi Volcano, Wangtian'e Volcano, and South Baotaoshan Volcano (Shi and Zhang, 2004; Zhao et al., 2004) (Figure 1a). Among these, Tianchi Volcano represents China's largest Cenozoic central-type composite stratovolcano (Li et al., 2006;Liu et al., 2015). The volcanic magmatic activity of Changbai Mountain can be categorized into three distinct stages: early-stage basaltic shield building, intermediate-stage trachytic cone formation, and late-stage ignimbrite eruptions (Fan et al., 2003; Wei et al., 2007). Shield-building stage initiated from about 25 Ma, dominated by upwelling of mantle-derived basaltic magma (Wei et al., 2013). Around 5 Ma, large-scale basaltic magma eruption occurred and shield lava plateaus formed at various volcanic vents. A thick and extensive cover layer developed in the upper crust and continuous eruptions ceased approximately 1.5 Ma. Cone-building Stage initiated from about 1.5 Ma. During Shield-building stage, the basaltic magma remained in the upper crust, followed by fractional crystallization and assimilation that further altered the composition of the magma. As a result,magma composition evolved to intermediate-acidic, more viscous trachytic magma. Trachytic magma erupted from Tianchi crater, forming the main body of Tianchi volcanic cone. During Late-stage Ignimbrite Eruption,Tianchi volcanic activity peaked again. Two major eruptions occurred in 4105 BC and 1199 AD which made pyroclastic deposits consolidated to form ignimbrite and overlaid the volcanic cone structure (Andreeva et al., 2018; Zhang et al., 2018; Zhang et al., 2018; Pan et al., 2020; Chen et al., 2021; Zhou et al., 2022).

The evolution of magma activity directly reflects the development of the subsurface magma chamber system. Consequently, the evolution of the Changbai Mountain subsurface magma reservoir system can also be divided into three distinct stages: (1) Early Stage (~25-5 Ma): A deep, small-scale mafic magma chamber formed at the crust-mantle boundary (~40 km depth). (2) Intermediate Stage (~5-1.5 Ma):Characterized by large-scale expansion of the mafic magma chamber at the crust-mantle boundary. (3) Late Stage (~1.5 Ma to present):Intermediate-acidic magma chambers formed and preserved in the shallow crust (Cheng et al., 2024; Chou et al., 2014; Zhu et al., 2019; Chen et al., 2021).

Thermal springs represent direct surface manifestations of geothermal activity. In the Changbai Mountain region, thermal springs are extensively developed, with six major thermal spring groups (Table 1) (Chen, 2015; Li. 2018; Li. 2015; Yan. 2016; Zhao. 2019). Among these thermal spring groups, the Hubin, Julong, and Jinjiang hot spring groups are distributed on the Tianchi volcano. These springs exhibit relatively high temperatures;The Shibadaogou, Xianrenqiao, and Laosandui hot spring groups are located farther from Tianchi Volcano. These springs emerge demonstrate slightly lower temperatures, generally below 60°C.

Table 1
Statistical data of Hot Springs in the Changbai Mountain Region.

Hot Spring	Amount	Longtitude	latitude	Temperature (°C)
Hubin Hot Spring Group	—	128°03′45"	42°01′12"	42-73
Julong Hot Spring Group	165	128°03′30"	42°02′27"	40-82
Jinjiang Hot Spring Group	108	127°59′33"	41°56′22	45-60
Shibadaogou Hot Spring Group	4	128°07′00"	41°25′04"	34-40
Xianrenqiao Hot Spring Group	7	127°11′12"	42°08′56"	44-62
Laosandui Hot Spring Group	26	126°48′15"	41°57′29"	30-35

3. Model and Method

3.1. Numerical model and simulation method

To simulate the evolution of the temperature field in the Changbai Mountain region under the influence of a magma chamber system, this study establishes a three-dimensional numerical model based on a three-dimensional crustal structure. For the length and width settings of the three-dimensional crustal model, the study area ranges from 41°E to 43°E (219 km) and from 127°N to 129°N (169 km). As for the depth of the three-dimensional crustal model, it is necessary to select a sufficiently deep range to accurately reflect the characteristics of the crustal temperature distribution and the influence of the magma chamber system on the regional temperature distribution. As a result, the model spans approximately 219 km in the north-south (NS) direction, 169 km in the east-west (EW) direction, and extends to a depth of 50 km. We employ the finite element method (FEM) using COMSOL Multiphysics software to conduct three-dimensional thermal conduction simulations. The model is discretized into 4,227,285 elements, and the thermal conduction process is simulated based on the three-dimensional Fourier heat conduction equation. The temperature calculations and the coupling of results are entirely performed within the software.

3.2. Three-dimensional geological model

Based on existing geological and geophysical data, including magnetotelluric,gravity, seismic data, this study establishes a three-dimensional geological model centered on the Changbai Mountain region (Figure 2). One of the models incorporates a magma chamber system to simulate the current thermal state of the Changbai Mountain area (Figure 2a), while the other model excludes the magma chamber system to serve as a comparative case for analyzing the influence of the magma chamber on the regional thermal state (Figure 2b). In the following sections, the model will be described in detail from four aspects: stratigraphic structure, magma chamber system, thermal properties of rocks, and temperature settings.

3.2.1. Lithospheric structure

The model is divided into the sedimentary layer, upper crust, middle crust, lower crust, and mantle. Surface elevation data were obtained from the SRTM database (https://earthexplorer.usgs.gov/), while the depths of the interfaces between these layers are obtained from density structure stratification based on gravity data (Choi et al., 2013), seismic wave velocity-derived crustal interface depths (Zhang et al., 2002), and the global crustal model Crust 1.0 (https://igppweb.ucsd.edu/~gabi/crust1.html). After incorporating these data into the model, interpolation methods were applied to fill in the gaps in the depth of each interface. Based on the analysis of previous geophysical studies in the Changbai Mountain region, the average Moho depth in the peripheral area of Changbai Mountain is 34 km, while in the Tianchi volcanic area, it is 40 km (Zhang et al., 2002; Guo et al., 2015; Li et al., 2022; Choi et al., 2013; Jiang, 2021). The average depth of the middle crust base is 26 km, and the middle-lower crust is primarily composed of Archean to Paleoproterozoic high-grade metamorphic rocks. The average depth of the upper crust base is 13 km, and the upper crust mainly consists of Jurassic granite intrusions with low porosity and permeability (Wu et al., 2002; Zhang et al., 2015). The average basement depth is approximately 4 km, overlain by a sedimentary layer composed of Sinian to Mesozoic sedimentary rocks and Cenozoic basalts. The area surrounding Tianchi Volcano is further covered by trachyte and ignimbrite. The Sinian to Mesozoic sedimentary rocks include clastic rocks and carbonates, with the great thickness, well-developed pores and fractures, and high permeability, making them the primary aquifer in the region and a favorable geothermal reservoir, with an average burial depth of 2–4 km (Cheng et al., 2024). The Cenozoic basalts are characterized by substantial thickness and widespread distribution but have poor porosity,

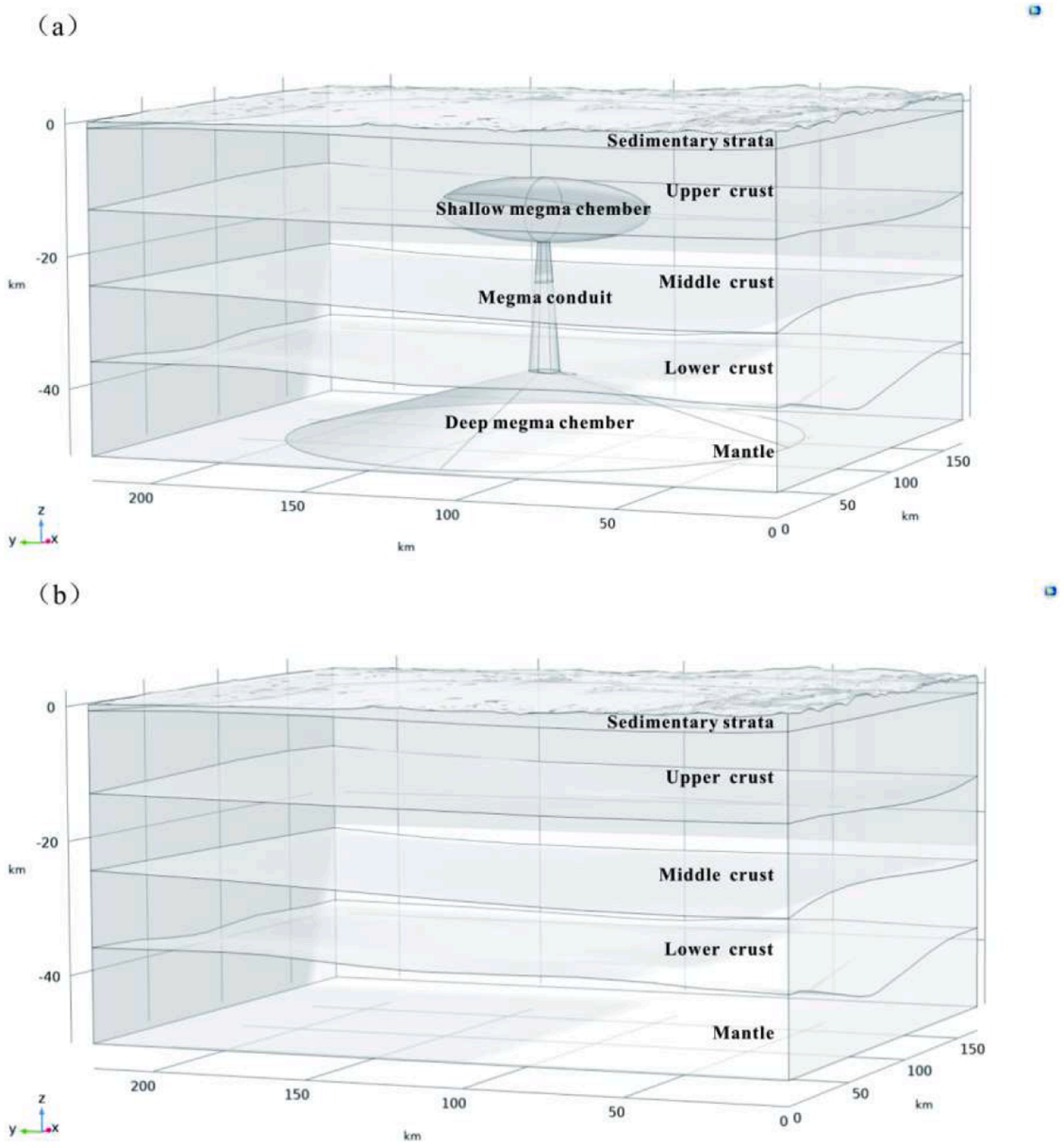

Figure 2. (a) Three-dimensional geological model of the Changbai Mountain region (including the magma chamber). (b) Three-dimensional geological model of the Changbai Mountain region (excluding the magma chamber).

permeability, and thermal conductivity, making them an effective cap rock.

3.2.2. *Magma chamber system*

Constructing a reasonable magma chamber system is crucial for the thermal modeling of volcanic geothermal systems. Previous studies, based on geophysical methods, have extensively investigated the magma chambers beneath the Changbai Mountain region, concluding that magma chambers exist both within the crust and the mantle. Therefore, this paper will discuss the magma chambers in Changbai Mountain by categorizing them into shallow magma chambers (crustal magma chambers) and deep magma chambers (mantle magma chambers).

First, it is essential to determine the subsurface morphology of the shallow and deep magma chambers. The process of magma intrusion is a critical constraint for understanding the evolution and subsurface state of magma chambers. To clarify the magma intrusion process under different crustal conditions, previous studies conducted three-dimensional thermodynamic simulations, obtaining models of magma intrusion under various conditions (Gorczyk and Vogt, 2018). The Changbai Mountain region exhibits both deep and shallow magma chambers, with the magma primarily being mantle-derived basaltic magma (Cheng et al., 2024; Chou et al., 2014; Zhu et al., 2019; Chen et al., 2021; Wei et al., 2013). In the corresponding models under these conditions, the deep magma chamber is approximately conical, the magma conduit is trapezoidal, and the magma chamber is elliptical. Therefore, this paper approximates the deep magma chamber, magma conduit, and shallow magma chamber as a cone, truncated cone, and ellipsoid, respectively, for three-dimensional modeling (Figure 2a).

The deep magma chamber is the result of the accumulation of mantle-derived basaltic magma at the crust-mantle boundary. According to seismic crustal tomography results, the depth of the deep magma chamber ranges from 38 to 65 km, with a horizontal extent of approximately 100-200 km (Guo et al., 1996; Guo et al., 2015; Zhu et al., 2019; Fan et al., 2020, 2021). These results are consistent with the depth of the deep magma chamber (30-60 km) derived from two-dimensional

magnetotelluric inversion (Chou et al., 2014) and the depth (42-56 km) obtained from mineralogical and geochemical methods (Chen et al., 2021). Based on these findings, this paper constructs a deep magma chamber model with a base diameter of 160 km and a depth of 40-50 km.

The shallow magma chamber is the result of the fractional crystallization, and assimilation of deep magma within the crust (Andreeva et al., 2018; Pan et al., 2020; Zhou et al., 2022). Different geophysical methods have yielded slightly varying results regarding the location and geometry of the shallow magma chamber. Based on artificial seismic methods, a large-scale low-velocity P-wave anomaly zone was identified at depths of 9-15 km beneath the Changbai Mountain region (Wang et al., 2002; Zhang et al., 2002). Seismic tomography also revealed a low-velocity P-wave anomaly zone at a depth of approximately 10 km beneath Tianchi (Yang et al., 2005). Jiang et al. (2023) used temperature data from four boreholes around Tianchi and performed numerical forward modeling to analyze the morphology of the shallow magma chamber, concluding that the best-fit model is an ellipsoid with a depth of 8–14 km, an east-west axis length of 20 km, and a north-south axis length of 70 km. Yan et al. (2023) identified a high Vp/Vs zone with an east-west axis length of approximately 30 km at a depth of about 10 km beneath Tianchi Volcano using high-precision seismic velocity data. Cheng et al. (2024) integrated multiple geophysical datasets to construct a two-dimensional profile model of the shallow magma chamber with a depth of 10-20 km and a length of 60 km. Based on these results, this paper constructs a shallow magma chamber model with an east-west axis length of 30 km, a north-south axis length of 70 km, and a depth of 10-20 km.

The most recent volcanic disturbance occurred between 2002 and 2005, during which previously blocked magma conduits were reopened by deep-source earthquakes, allowing deep magma to reconnect with the shallow magma chamber through the conduits (Liu et al., 2020; Zhang et al., 2024). Based on thermodynamic simulations of magma intrusion under corresponding conditions (Gorczyk and Vogt, 2018), this paper constructs a magma conduit model with a base radius of 5 km and a top radius of 2 km.

3.2.3. Rock thermal properties

The stratigraphy of the Changbai Mountain region is well-developed, with outcrops exposed throughout the surrounding area. The basement of the Changbai Mountain region primarily consists of Archean to Meso-Neoproterozoic metamorphic rocks and Mesozoic granites. Overlying the basement, the Paleozoic strata include the Sinian, Cambrian, Ordovician, Carboniferous, and Permian systems, while the Mesozoic strata comprise the Triassic, Jurassic, and Cretaceous systems. The Cenozoic strata consist of the Tertiary and Quaternary systems. To supplement the thermal property data of rocks in the Changbai Mountain region, this study measured the thermal conductivity of 93 outcrop samples and tested the heat production rate of 42 of these samples. The thermal conductivity of the rocks was tested using the transient plane source method at the National Key Laboratory of Petroleum Resources and Engineering at China University of Petroleum (Beijing). The test results are presented in Table 2:

The heat production rate measurements of the samples were conducted at the Analytical Laboratory of the Beijing Research Institute of Uranium Geology, China National Nuclear Corporation. The concentrations of uranium (U) and thorium (Th) were determined using NexION300D inductively coupled plasma mass spectrometer (ICP-MS) under controlled laboratory conditions of 20.1°C and 19% relative humidity. Potassium (K) content was measured using a Z-2000 atomic absorption spectrophotometer at 21.1°C and 28% relative humidity. The results of the rock heat production rate measurements are presented in Table 3.

Based on measured rock thermal property data and previous research findings, the thermal properties of each stratum in the three-dimensional geological model of Changbai Mountain were calculated.

Table 2
Thermal Conductivity Column of the Changbai Mountain Region.

Stratum	Sample	Thermal Conductivity (W/(m·K))	Average Thermal Conductivity (W/(m·K))
Quaternary	Basalt (4)	1.3-2.1	2.65
	Quartz sandstone (6)	1.85-7.03	
	Siltstone (1)	3.58	
	Shale (3)	1.75-3.65	
	Trachyte (1)	1.75	
Neogene	Basalt (11)	1.37-2.88	1.63
Cretaceous	Sandstone (6)	1.30-2.61	2.19
	Granite (4)	2.76-2.92	
Jurassic	Andesite (3)	1.54-2	2.44
	Tuff (4)	2.16-3.05	
	Sandstone (4)	2.0-3.74	
	Mudstone (1)	2.22	
	Granite (1)	2.88	
Triassic	Andesite (3)	1.92-4.27	2.56
	Sandstone (1)	2.31	
Permain	Granite (6)	1.86-3.16	2.83
	Siltstone (1)	3.36	
Carboniferous	Siltstone (1)	3.16	2.82
	Coal (1)	2.47	
Ordovician	Limestone (1)	4.98	4.98
Cambrian	Dolomite (2)	2.15-2.94	2.82
	Limestone (2)	3.18-3.46	
	Siltstone (1)	3.5	
	Shale (1)	1.9	
Sinian	Limestone (3)	2.63-4.62	3.41
Proterozoic-Archaean	Gneiss (7)	1.32-3.09	2.91
	Granite (9)	2.44-3.16	
	Schist (1)	2.56	
	Marble (2)	4.37-5.09	
	Gabbroite (1)	2.8	
	Phyllite (1)	2.14	

(Samples listed with the number of samples in parentheses)

The sedimentary layer is primarily composed of Sinian-Mesozoic sedimentary rocks and Cenozoic basalt, with thermal property data derived from measured thermal properties and thermal property data of sedimentary basins such as the Songliao Basin (Tang et al., 2024; Li, 2023; Fuchs, 2018). The thermal property data of the upper crust granitic intrusions are sourced from measured granite thermal properties and previous studies on the thermal properties of deep-seated granites (Qiu, 2002; Xiang et al., 2022; Sun et al., 2019). The thermal properties of the middle and lower crust are based on measured metamorphic rock thermal properties and previous research on the thermal properties of deep-seated metamorphic rocks (Tiskatine et al., 2023; Merriman et al., 2013; Shakirov et al., 2021; Choi et al., 2013; Zhang et al., 2002; Jiang, 2017). The mantle thermal properties are referenced from measured basalt thermal properties and related results from previous studies (Merriman et al., 2013; Cheng et al., 2024; Wang et al., 2023; Okuda et al., 2020; Xia et al., 2020). Finally, the thermal property data for each part of the model were obtained (Table 4):

3.2.4. Temperature setting

Based on the average surface temperature of the Changbai Mountain region, the surface temperature of the model is set to 10°C. The bottom temperature of the model is constrained by the Moho temperature, which plays a critical role in regulating magmatic activity. According to thermodynamic simulation results, 1050 K and 1100 K can be considered as two critical values for the Moho temperature (Tmoho) in the context of magmatic activity, as the state of magma undergoes significant changes within this 50 K range. When Tmoho<1050 K, magma can erupt rapidly to the surface; when Tmoho=1050 K, magma reaches a depth close to the surface; at Tmoho=1075 K, magma uplifts the lower crust vertically without penetrating the upper crust; at Tmoho=1090 K, basaltic magma enters the upper crust to form secondary magma chambers, with some magma reaching the surface; at Tmoho = 1100 K,

Table 3
Heat production rate Column of the Changbai Mountain Region.

Stratum	Sample	Average Density (kg/m^3)	Heat Production ($\mu W/m^3$)	Average Heat Production ($\mu W/m^3$)
Quaternary	Basalt (1)	2690	0.73	1.65
	Sandstone (2)	2620	0.42-1.82	
	Shale (1)	2680	2.02	
	Trachyte (1)	2540	3.24	
Neogene	Basalt (2)	2480	0.27-0.98	0.63
Cretaceous	Sandstone (3)	2720	0.82-1.56	1.86
	Granite (2)	2540	1.28-4.08	
Jurassic	Andesite (1)	2710	0.64	1.09
	Tuff (1)	2710	0.91	
	Sandstone (1)	2380	0.3	
	Granite (1)	2670	2.51	
Triassic	Andesite (1)	2610	2.18	2.04
	Sandstone (1)	2680	1.9	
Permain	Granite (5)	2585	0.78-2.57	1.42
	Siltstone (1)	2500	0.93	
Carboniferous	Siltstone (1)	2730	2.57	2.57
Ordovician	Limestone (1)	2820	0.18	0.18
Cambrian	Limestone (2)	2710	0.32-2.91	1.98
	Siltstone (1)	2720	1.84	
	Shale (2)	2790	1.91-2.91	
Sinian	Limestone (1)	2550	0.88	0.88
Proterozoic-Archaean	Gneiss (1)	2590	1.69	1.43
	Granite (5)	2600	0.54-2.81	
	Schist (1)	2810	2.35	
	Marble (1)	2830	0.04	
	Gabbroite (1)	2630	1.16	
	Phyllite (1)	2800	0.18	

(Samples listed with the number of samples in parentheses)

Table 4
Thermal Properties of Rocks in Each Layer of the 3D Model.

Layers	Density (kg/m^3)	Counductivity (W/(m· K))	Heat Production ($\mu W/m^3$)
Sedimentary Layer	2600	2.57	1.25
Upper crust	2670	2.88	2.34
Middle crust	2800	2.81	1.11
Lower crust	2900	2.32	0.39
Mantle	3250	3.03	0.33

secondary magma chambers remain in the upper crust; and when Tmoho > 1100 K, as the Moho temperature increases, the crustal strength decreases, and magma only extends at the base of the lower crust (Gorczyk and Vogt, 2018). Currently, although volcanic activity persists in the Changbai Mountain region, there is no magma eruption. Geophysical evidence confirms the presence of shallow magma chambers in the area, which aligns with the magmatic activity state simulated at Tmoho = 1100 K. Therefore, this study adopts Tmoho = 1100 K (≈827°C) as the Moho temperature. To estimate the temperature at the model's lower boundary, a geothermal gradient must be assigned from the Moho to the lower boundary. Based on the Moho depth and the temperature difference between the Moho and the surface, the overall geothermal gradient of the model is estimated to be approximately 25°C/km, which is used as the geothermal gradient below the Moho to calculate the lower boundary temperature.

The temperature of magma chambers is discussed separately for shallow and deep magma chambers. This study employs an empirical equation based on the SiO_2 content of volcanic rocks to preliminarily estimate the temperatures of shallow and deep magma chambers (Equation 1), as follows (Duan et al., 2022):

$$T = -14.16 * w + 1723 \quad (1)$$

Where the T is temperature, in °C;w is the mass fraction of SiO_2, %.

According to previous studies, the average SiO_2 content (wt%) of erupted rocks from the shallow magma chamber in the Changbai Mountain region is approximately 67%, while that of the deep magma chamber is around 50% (Yi et al., 2021). Based on these values, the temperature of the shallow magma chamber in Changbai Mountain is estimated to be approximately 775°C, and the deep magma chamber is estimated to be around 1015°C. Zhang et al. (2017) utilized the relationship between electrical conductivity and temperature to estimate the temperature of the shallow magma chamber in the Changbai Mountain region to be 723-756°C. Additionally, Cheng et al. (2024) inferred the temperature of the deep magma chamber in the Changbai Mountain region to be approximately 1050°C by considering the melting temperatures of major mantle minerals in the upper mantle. In this study, the temperature of the shallow magma chamber is set to 750°C, and the temperature of the deep magma chamber is set to 1050°C.

3.2.5. *Thermal storage properties*

In previous studies, it has been proposed that the carbonate rock layer at a depth of 2–4 km in the Changbai Mountain region exhibits significant total thickness, well-developed pores and fractures, and high permeability, making it the primary aquifer in the area and a favorable hydrothermal reservoir (Cheng et al., 2024). In this study, the depth interval of 2–4 km is selected as the target layer for calculating the geothermal resource potential. The properties of the formation are derived from measured sample data and relevant data from previous studies (Fuchs, 2018; Miao et al., 2014; Cheng et al., 2024). While the specific heat capacity and density of water can significantly deviate from the standard state due to temperature variations, this study employs the Water Equation of State IAPWS-97 (2012) (https://iapws.org/relguide/IF97-Rev.pdf) to correct the density and specific heat capacity of water in the thermal reservoir. The calculations were performed at the average reservoir temperature of 138.4 °C and average reservoir pressure of 81 MPa, the resulting parameters are summarized in Table 5.

4. Result

This study calculates the surface heat flow and subsurface temperature distribution in the Changbai Mountain region under two models: with and without the presence of magma chambers. By comparing the results of the two models, the influence of the magma chamber system on the temperature and heat flow distribution in the Changbai Mountain region is analyzed. Based on the differences in temperature and heat flow, the potential of the magma chambers as a geothermal reservoir and the additional heat contribution to the Changbai Mountain region are quantified. The specific results are as follows.

Table 5
Related parameters of heat storage calculation.

	Density of storage (kg/m^3)	Porosity (%)	Specific heat capacity of storage (J/(kg·°C))	Density of water (kg/m^3)	Specific heat capacity of water (J/(kg·°C))
Geothermal reservoir	2700	3.1	715	971.7	4285

4.1. Temperature

According to the three-dimensional Fourier heat conduction equation, we obtained the three-dimensional temperature distribution of the Changbai Mountain region (Figure 3). To analyze the temperature distribution characteristics of the region, two profiles, AA' and BB', were selected for detailed analysis (Figure 4a, b), enabling the observation of the three-dimensional temperature distribution in the EW and NS directions, respectively. The results indicate that due to the continuous thermal influence of the magma chambers, the surrounding areas experienced significant temperature increases, while the temperature in the peripheral regions far from the magma chambers remained relatively stable, showing almost no effect from the thermal influence of the magma chambers. To further analyze the impact of the magma chambers on the distribution of shallow geothermal resources, temperature curves at depths of 1 km to 5 km were plotted for both profiles (Figure 4c, d). From the figure 4, it can be observed that the temperature at a buried depth of 1 km ranges from 40.°C to 64.8°C; at 2 km buried depth, the temperature ranges from 67.8°C to 119.7°C; at 3 km buried depth, the temperature ranges from 101.6°C to 175.2°C; at 4 km buried depth, the temperature ranges from 132.5°C to 235.2°C; and at 5 km buried depth, the temperature ranges from 163.3°C to 290.5°C.

The thermal influence of the magma chambers provides the potential for the existence of deep high-temperature geothermal resources. According to national geothermal resource evaluation methods and estimation guidelines, geothermal resources with temperatures exceeding 150°C are generally considered suitable for geothermal power generation, and the shallower the depth of these high-temperature resources, the higher the economic benefits of their exploitation. Both the AA' and BB' profiles show that the temperature at a depth of 3 km in the central Changbai Mountain region exceeds 150°C. These results demonstrate the region's significant potential for hosting high-temperature geothermal resources.

To evaluate the distribution of high-temperature geothermal resources, a map of the depth of the 150 °C isotherm surface was plotted (Figure 5). In the Changbai Mountain region, the buried depth of the 150 °C isotherm ranges from 2.35 km to 4.43 km. The shallowest depths are observed in and around the areas where magma chambers are distributed, with an average depth of 2.73 km. The overall average depth for the entire region is 3.82 km, indicating significant potential for high-temperature geothermal resources.

4.2. Surface heat flow

Based on the temperature simulation results of the model, the surface heat flow of the model was calculated. To more clearly contrast the additional heat flow brought by the magma chambers to the region, this study also calculated the surface heat flow of the model without magma chambers (Figure 6). In the presence of the magma chamber, the surface heat flow in the Changbai Mountain region ranges from 70.1 to 130.8 mW/m^2, with an average heat flow of approximately 86.2 mW/m^2. In the absence of the magma chamber, the surface heat flow in the Changbai Mountain region ranges from 61.8 to 91.3 mW/m^2, with an average heat flow of approximately 75.9 mW/m^2. On average, the magma chamber contributes an additional heat flow of approximately 10.3 mW/m^2 to the region.

4.3. Geothermal resource potential

The three-dimensional numerical model contains extensive temperature data. To improve the accuracy of geothermal resource potential estimation, this study proposes a method for calculating regional geothermal resources based on numerical simulation. This method first selects suitable geological formations as reservoirs based on the properties of each sedimentary layer, determining the burial depth and spatial distribution of the reservoirs. Subsequently, a triple integral over the temperature field within the reservoir region is performed, and the integral method is applied to calculate the geothermal resource potential contained in the reservoirs (Equations 2 and 3).

$$R = (t_r - t_0)(\rho_r c_r(1-\varphi) + \rho_w c_w \varphi) \tag{2}$$

$$Q = \int_{\Omega}\int\int R dv \tag{3}$$

Where Q is the heat stored in the reservoir, in J; ρ_r is the density of the reservoir rock, in kg/m^3; c_r is the specific heat capacity of the reservoir rock, in J/(kg·°C); φ is the porosity of the reservoir rock, %; t_r is the temperature of the reservoir, in °C; t_0 is the surface temperature, in °C; ρ_w is the density of geothermal water, in kg/m^3; c_w is the specific heat capacity of water, in J/(kg·°C); Ω is the volume of the reservoir calculation region, in m^3; dv is the volume element of the region, in this study, the volume element is defined as the product of coordinate differentials

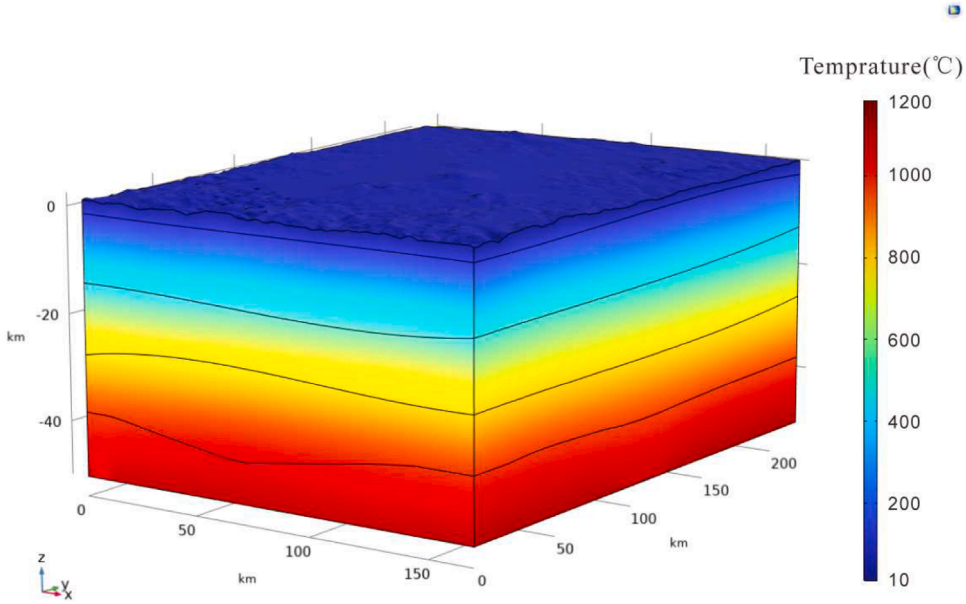

Figure 3. The three-dimensional temperature distribution in the Changbai Mountain area.

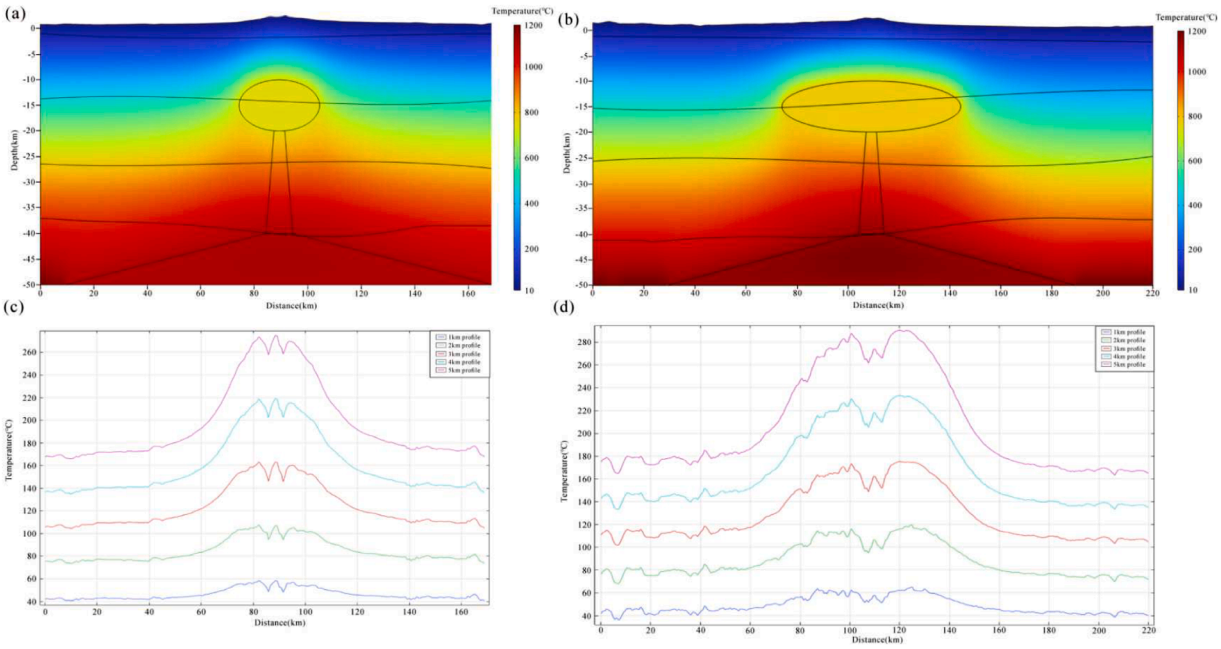

Figure 4. (A) Temperature field distribution of BB 'profile (b) Field distribution of AA' profile (c) BB ' temperature profile-1～ -5km (d) AA' temperature profile-1～ -5km.

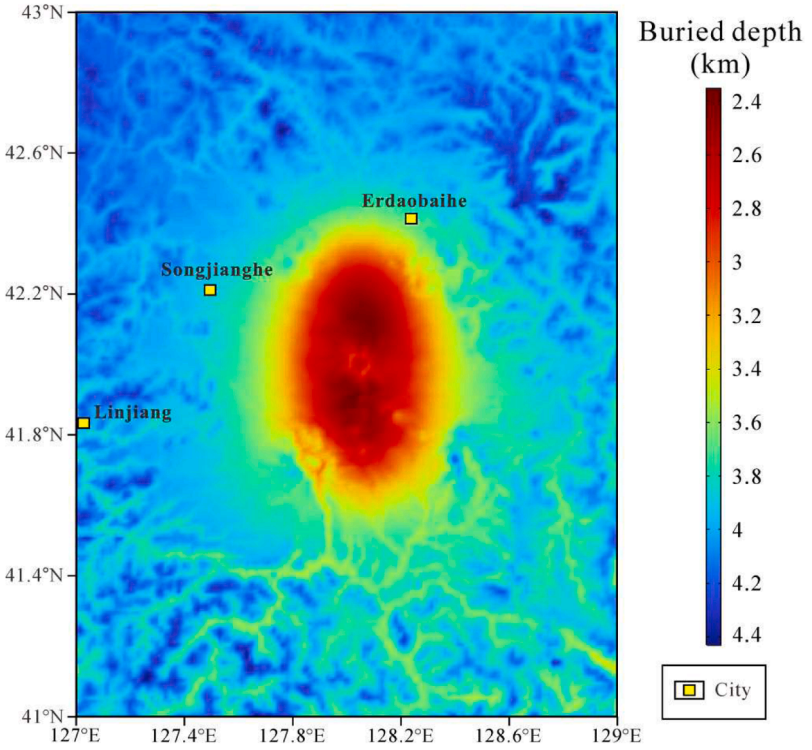

Figure 5. 150°C isotherm surface in Changbai Mountain.

in the coordinate system, i.e.,dv=dxdydz.

Based on the investigation of the stratigraphic structure in the Changbai Mountain region, this study selects the carbonate rock formations at a depth of 2-4 km as the reservoir and evaluates the geothermal resource potential using the aforementioned method. In the model with a magma chamber, the geothermal resource potential in the Changbai Mountain region is approximately 5.79×10^{20}J; in the model without a magma chamber, the geothermal resource potential is approximately 5.57×10^{20}J. The difference in geothermal resource potential attributed to the magma chamber is approximately 2.25×10^{21}J.

Within the 2-4 km depth interval, the geothermal temperatures in the Changbai Mountain region are mostly above 150 °C, making it a suitable high-temperature geothermal reservoir for power generation. Therefore, this study further estimates the geothermal power generation potential of the Changbai Mountain region. Generally, for geothermal power

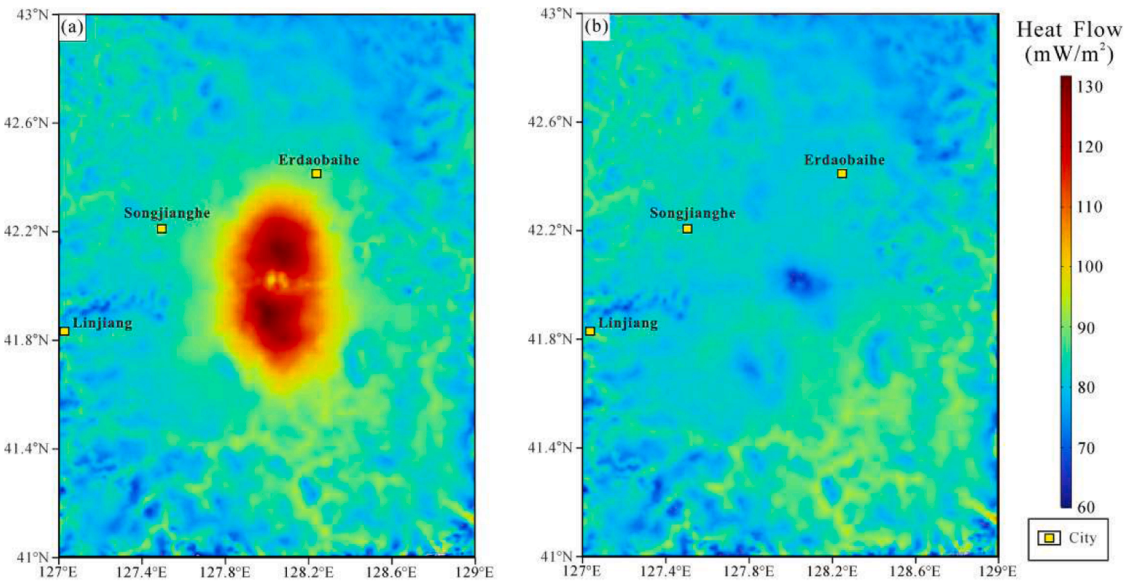

Figure 6. (A) Surface heat flow in Changbai Mountain region (with magma chamber) (b) Surface heat flow in Changbai Mountain region (without magma chamber).

generation, the evaluation of its potential requires converting the geothermal resource potential using a recoverable heat rate and power generation rate, which serves as the reservoir's power generation potential (Equation 4) (Williams et al., 2008).

$$E_e = R_q R_e Q \tag{4}$$

Where E_e is the electrical energy that can be generated based on the resource assessment, in J; Q is the heat stored in the reservoir, in J; R_q is the recoverable heat rate, R_e is the power generation rate. .

To assess the geothermal power generation potential in the Changbai Mountain region, it is necessary to assume the geothermal production period and the production time. This study assumes that the geothermal reservoir in the Changbai Mountain region can sustain geothermal extraction for 50 years, with an annual production time of 8,000 hours. Based on these conditions, the geothermal power generation potential of the Changbai Mountain region is calculated.

In previous studies, the value of the recoverable heat rate R_q is often related to the flow state of fluids in the reservoir. If the fluid flow is primarily controlled by fracture permeability, R_q is typically taken as 0.08-0.2; if the fluid flow is controlled by matrix permeability, R_q is usually taken as 0.1-0.25 (Williams et al., 2008). In this study, the selected reservoir is a carbonate rock formation. Based on the measured porosity of carbonate rock samples in the region and previous research, the porosity of carbonate rocks in the Changbai Mountain region is relatively low, but fractures are well-developed (Cheng et al., 2024; Wang, 2023; Zhao, 2019). Therefore, this study concludes that the fluid flow in this reservoir is primarily controlled by fracture permeability, and the recoverable heat rate is taken as the average value for fracture-controlled flow, i.e., 0.14. The value of the power generation rate R_e is taken as the world average conversion rate, i.e., 0.12 (Zarrouk et al., 2014). Substituting these rates into Equation 4, the geothermal power generation potential of the Changbai Mountain region is estimated to be approximately 6759.4 MWe, with the additional power generation potential attributed to the magma chamber being approximately 262.4 MWe, indicating significant geothermal power generation potential.

To validate the geothermal resource potential calculation method proposed in this study, the average temperature of the reservoir in the numerical model is used as the reservoir temperature, and the geothermal reservoir volume method is applied to calculate the geothermal resource content of the reservoir (Equation 5).

$$Q = AZ(t_r - t_0)(\rho_r c_r(1-\varphi) + \rho_w c_w \varphi) \tag{5}$$

Where Q is the heat stored in the reservoir, in J; A is the area of the reservoir, in m^2; Z is the thickness of the reservoir, in m; ρ_r is the density of the reservoir rock, in kg/m^3; c_r is the specific heat capacity of the reservoir rock, in J/(kg·°C); φ is the porosity of the reservoir rock, %; t_r is average the temperature of the reservoir, in °C; t_0 is the surface temperature, in °C; ρ_w is the density of geothermal water, in kg/m^3; c_w is the specific heat capacity of water, in J/(kg·°C).

According to the geothermal reservoir volume method, the geothermal resource potential in the Changbai Mountain region is calculated to be approximately 1.52×10^{20} J in the model with a magma chamber. This result is lower than the value obtained in this study, primarily because the geothermal reservoir volume method assumes that the temperature is uniform throughout the three-dimensional region of the reservoir, typically using the average reservoir temperature for geothermal resource calculations. However, in reality, the temperature within the reservoir is a three-dimensional function of the region's length, width, and depth, with each point having a corresponding temperature. In the Changbai Mountain region, temperature fluctuations are significant, with the maximum temperature difference at the same depth within the 2-4 km range reaching 102.7°C. Using the average reservoir temperature to represent the temperature at all points in the reservoir imposes significant constraints on the calculation, resulting in lower reliability of the results. Zuo et al. (2024), based on their proposed multi-data fusion method for calculating geothermal resources in sedimentary basins, integrated the geothermal resource potential of various reservoirs in the Sichuan Basin and obtained more accurate results, demonstrating that integral calculations can provide higher credibility for geothermal resource assessments. In this study, the three-dimensional numerical simulation model is used to finely characterize the temperature distribution within the selected reservoir, and a triple integral of the reservoir temperature is performed. By replacing the average calculation of the geothermal reservoir volume method with integral calculations, the results achieve higher accuracy.

5. Discussion

5.1. Comparison Between Numerical Simulation Results and Measured Data

To validate the accuracy of the numerical simulation results, this study compares the simulated temperature data with measured geothermal well temperature data from the Changbai Mountain region. There are four geothermal wells with temperature measurement data in the area (Jiang et al., 2023): C-1, located near the Tianchi Volcano of Changbai Mountain, and C-2, C-3, and C-4, situated in its vicinity (Figure 1). The temperature profiles from these wells and the corresponding numerical simulation curves are shown in Figure 7.

From the temperature profiles, it is evident that the simulated temperature curves for wells C-2, C-3, and C-4 exhibit a high degree of overlap with the measured temperature curves. However, due to the presence of thermal convection effects in these wells, the simulated temperature curves diverge from the measured curves in regions affected by thermal disturbances. Well C-1, located near the Tianchi Volcano of Changbai Mountain, experiences extremely strong thermal convection and has a relatively shallow depth. The intense thermal disturbances in this well make its shallow measured geothermal gradient and heat flux unrepresentative of the full-depth temperature evolution trend and heat flow at this location. Therefore, this study primarily focuses on comparing the temperature profiles of wells C-2, C-3, and C-4

Table 6
Comparison of surface heat flow and geothermal gradient.

Well	Measured heat flow (mW/m^2)	Caculated heat flow (mW/m^2)	Measured temperature gradient (°C/km)	Caculated temperature gradient (°C/km)
C-1	270±6	126.3	163.4±0.1	61
C-2	77±5	84.6	29.13±0.1	32.9
C-3	76±1	85.3	31.25±0.1	34.3
C-4	78±4	89.6	21.7±0.1	25.9

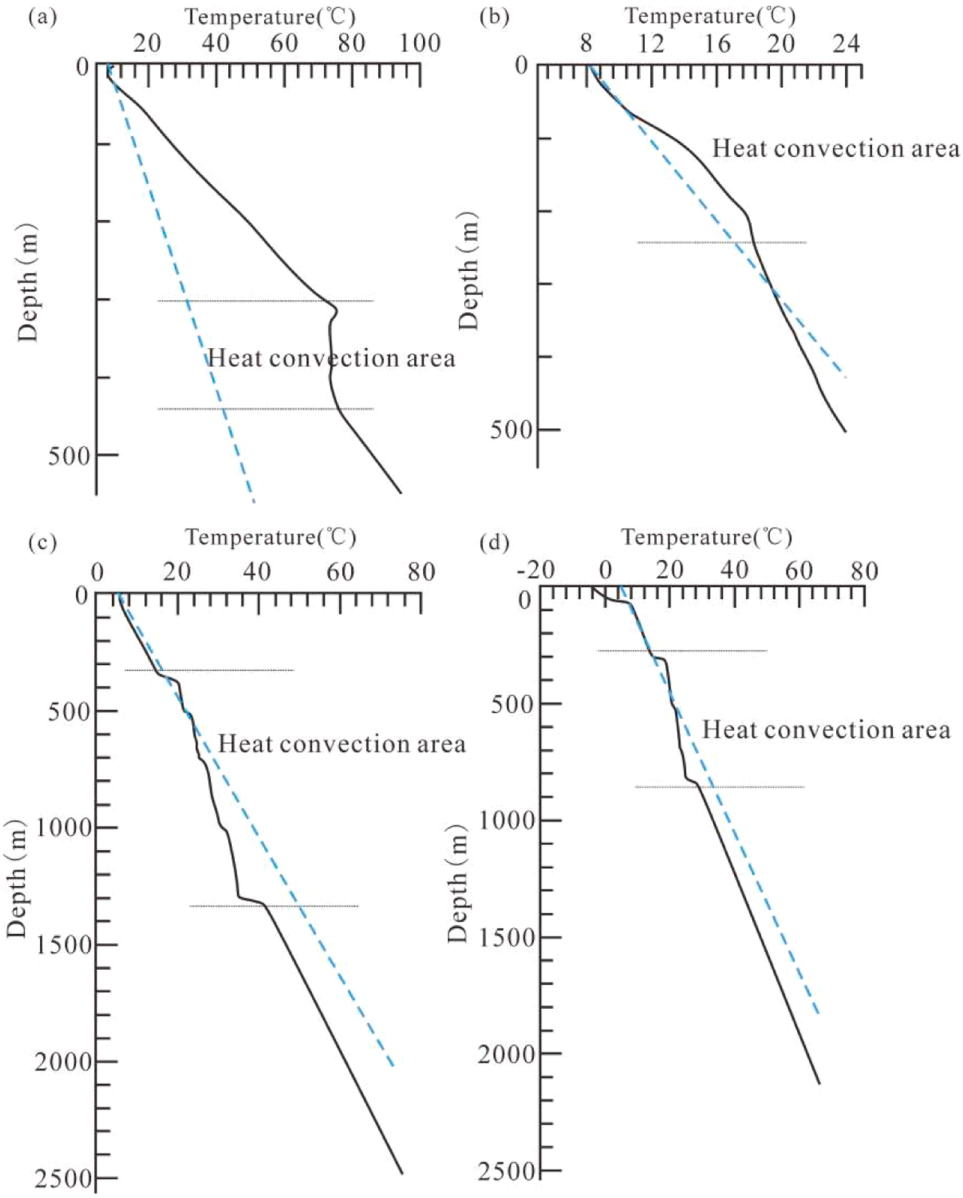

Figure 7. Comparison Between Measured Temperature Curves and Numerical Simulation Curves.
(The black solid line represents the measured temperature curve, the blue dashed line represents the numerical simulation curve. (a) Well C-1, (b) Well C-4, (c) Well C-2, (d) Well C-4).

with the simulation results. The relevant data comparison is presented in Table 6.

For wells C-2, C-3, and C-4, the numerical simulation results closely match the measured data, with the calculated heat flow and geothermal gradient being slightly higher than the measured values. These discrepancies arise from the relatively weak thermal convection effects in the regions where these wells are located. For the majority of the area where the thermal conduction method is applicable, the numerical simulation results are in close agreement with the measured data, demonstrating strong reliability and credibility.

For the overall surface heat flow in the Changbai Mountain region, previous studies have also conducted relevant research. Jiang et al. (2016) added two high-quality surface heat flow data points for the Changbai Mountain region, both located west of the Tianchi Volcano. The measured surface heat flow values were 79.9 mW/m^2 and 70.9 mW/m^2, respectively. Jiang (2021) based on over 4,000 global surface heat flow data points and deep learning algorithms, estimated the surface heat flow in the Changbai Mountain region to be around 84 mW/m^2. These results are close to the surface heat flow values obtained from the numerical simulations in this study, thereby demonstrating the accuracy and reliability of the numerical simulation results presented in this study.

5.2. *Influence Range of the Magma Chamber system on the Changbai Mountain*

Magmatic activity plays a crucial role in influencing the temperature and fluid flow of volcanic geothermal systems. The continuous heating from magmatic activity can sustain geothermal fluids in volcanic geothermal systems at temperatures exceeding 100°C (Traineau et al., 1989; Stefánsson, 2017; Karingithi et al., 2010). Under such conditions, magmatic activity is generally the dominant factor controlling the formation and distribution of geothermal resources in volcanic geothermal systems. The Changbai Mountain region exhibits active magmatic activity, with large-scale magma chambers present in both the crust and mantle. To analyze the influence range of the magma chambers on the region and the extent of their impact within this range, this study examines the temperature distribution along profiles AA' and BB' and compares the terrestrial heat flow differences between models with and without magma chambers, thereby assessing the influence of magma chambers on regional temperature and heat flow.

From the temperature profiles (Figures 8a and 8b), it is evident that the shallow magma chamber significantly elevates the temperature in its surrounding areas, both vertically and horizontally. In contrast, the deep magma chamber, due to its temperature being closer to that of the mantle, does not exhibit a noticeable temperature increase in its vicinity. For temperature curves at different depths (Figures 8c and 8d), the shallow magma chamber shows a similar influence horizontally. In profile BB', the temperature curves at all depths exhibit a sharp increase at a distance of 35 km from the edge of the shallow magma chamber. In profile AA', the temperature curves at all depths show a sharp increase at a distance of 40 km from the edge of the shallow magma chamber. Both profiles demonstrate that the closer the distance to the shallow magma chamber, the faster the temperature rises, and within the distribution range of the shallow magma chamber, the temperature changes more gradually. Vertically, the deeper the depth, the greater the temperature increase.

From the perspective of surface heat flow, the influence range of the magma chamber system on heat flow is similar to its influence on temperature (Figure 9). Specifically, in profile BB', the terrestrial heat flow exhibits a sharp increase at a distance of 35 km from the edge of the shallow magma chamber. In profile AA', the terrestrial heat flow shows a sharp increase at a distance of 40 km from the edge of the shallow magma chamber. Additionally, the closer the proximity to the shallow magma chamber, the greater the difference in surface heat flow, with the difference reaching its peak within the distribution range of the shallow magma chamber.

To evaluate the influence range of the magma chamber on the regional geothermal system, this study plotted the distribution of surface heat flow differences between models with and without a magma chamber (Figure 10a). From the figure, it is evident that the influence of the magma chamber on surface heat flow gradually decreases from the

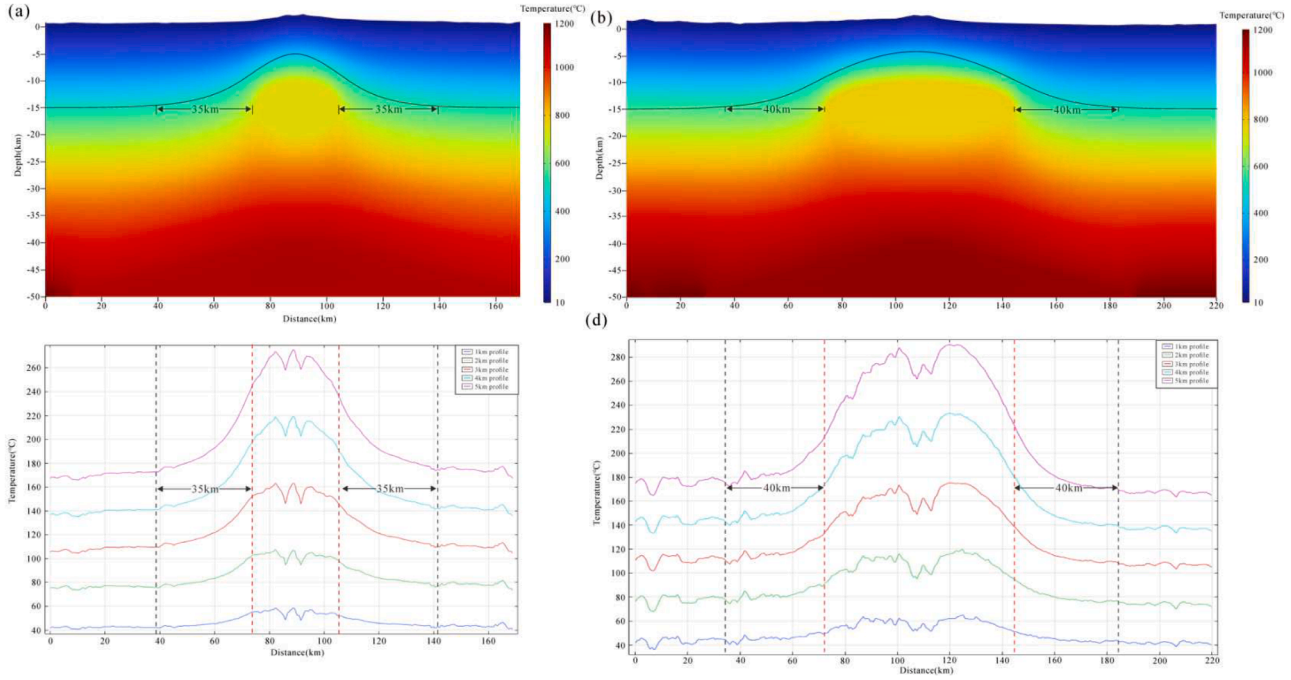

Figure 8. (a) Influence range of the magma chamber on temperature along profile BB'; (b) Influence range of the magma chamber on temperature along profile AA'; (c) Influence range of the magma chamber on temperature at depths of -1 to -5 km along profile BB'; (d) Influence range of the magma chamber on temperature at depths of -1 to -5 km along profile AA';.

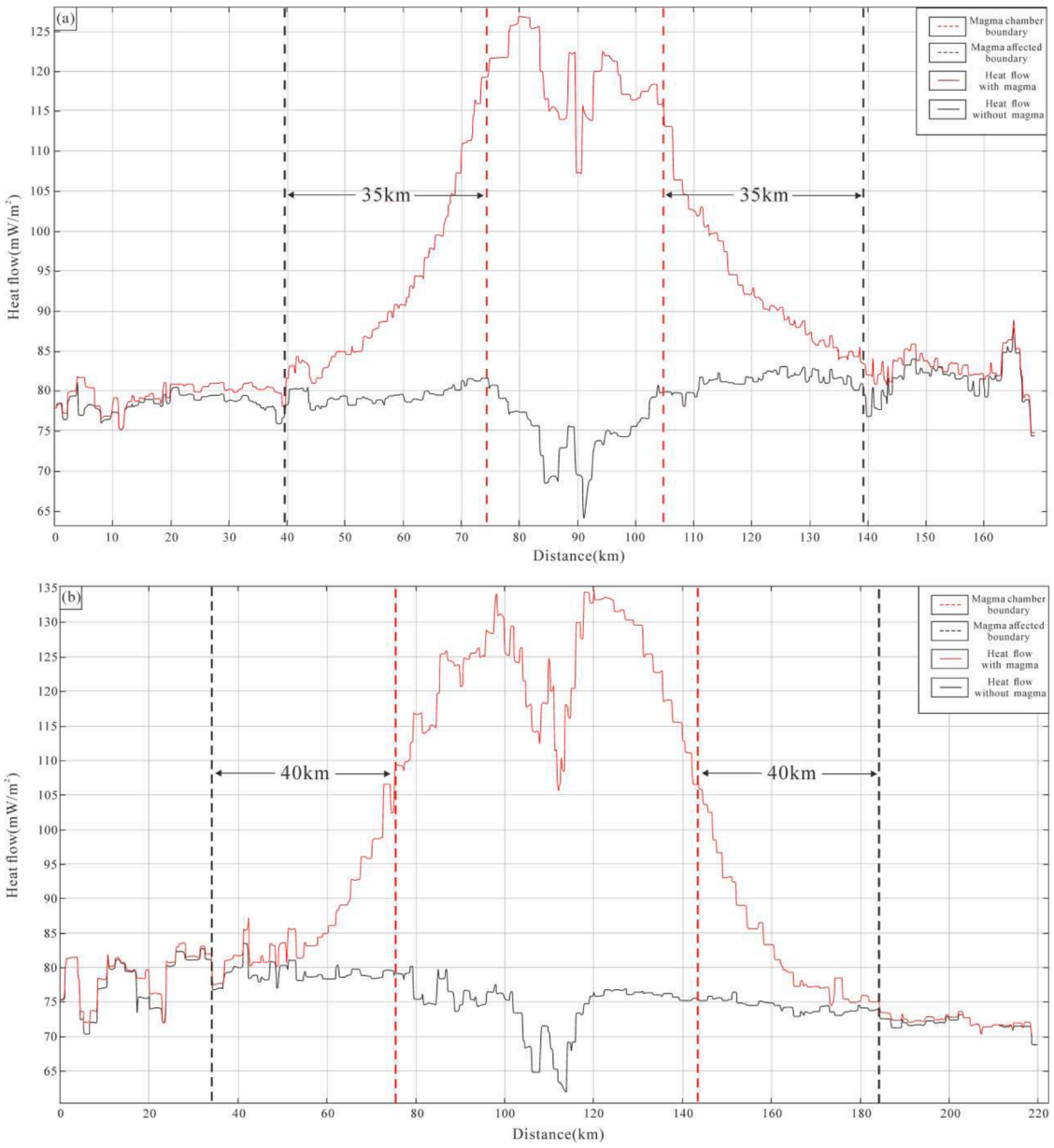

Figure 9. (a) Surface heat flow differences along profile BB'; (b) Surface heat flow differences along profile AA'.

center toward the periphery. To discuss the influence range of the magma chamber on the geothermal system in the Changbai Mountain region, the 2 mW/m^2 contour line of the heat flow difference was selected as the boundary of the magma chamber's influence range, delineating its impact on the region (Figure 10b). As can be seen from Figure 10b, the influence range of the magma chamber system extends approximately 100 km in the east-west (EW) direction and 150 km in the north-south (NS) direction, covering an area of approximately 11,780 km^2. Although the magma chamber has different lengths in the EW and NS directions, the extent of its outward influence is nearly the same, approximately 40 km in both directions. This result indicates that the outward influence range of the magma chamber is almost unaffected by its shape. Meanwhile, the hot spring groups in the Changbai Mountain region are all distributed within the influence range of the magma chamber system, with most located within the range of the magma chamber itself. Based on this, this study speculates that the magma chamber system in the Changbai Mountain region has facilitated the formation of the area's hot spring groups. The continuous heating from the shallow magma chamber provides an additional heat source to the groundwater, creating a greater temperature difference between the groundwater and the recharge water from surface. This promotes the thermal convection effect in the Changbai Mountain region, leading to the formation of numerous hot spring groups on the surface.

6. Conclusion

(1) The magma chamber system contributes significant additional heat to the surrounding region, with the shallow magma chamber having a much greater impact than the deep magma chamber. The influence area covers approximately 11,780 km^2, extending about 100 km in the east-west (EW) direction and 150 km in the north-south (NS) direction. While the influence range is related to the shape of the magma chamber, the outward radiation range is approximately 40 km in all directions, which is almost unaffected by its shape. Within the influence range, temperature and heat flow increase sharply from the periphery toward the center, reaching their peak within the distribution range of the shallow magma chamber. These results show a strong correlation with the

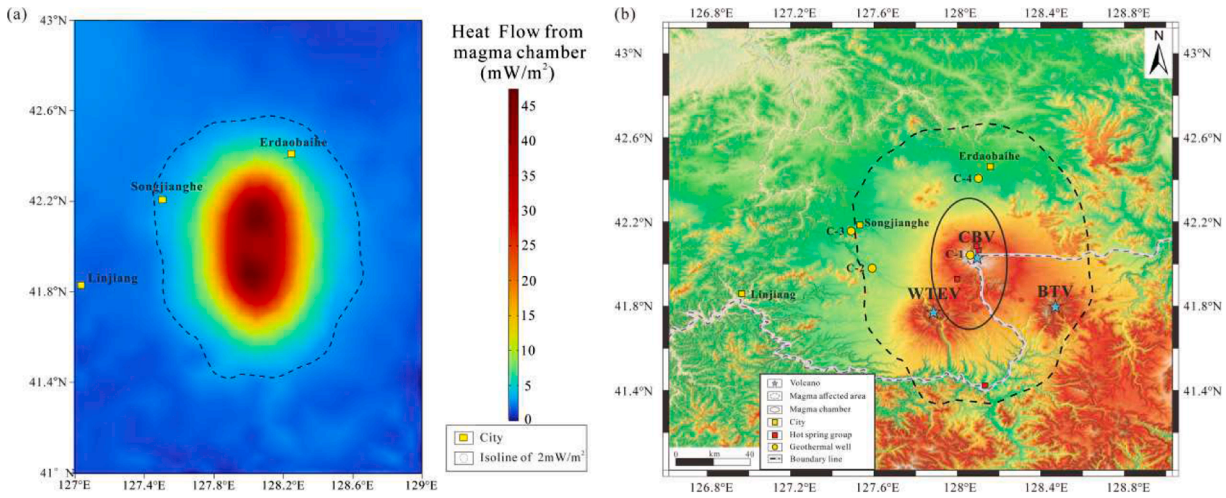

Figure 10. (a) Heat flow distribution brought by magma chamber (b) Impact range of magma chamber on the geothermal field in Changbai Mountain area.

distribution of hot springs and geothermal wells, demonstrating high credibility.

(2) The continuous heating from the magma chamber system makes the presence of deep high-temperature geothermal resources in the Changbai Mountain region possible. On average, the magma chamber system contributes an additional heat flow of approximately 10.3 mW/m² to the region. The depth of the 150°C isotherm ranges from 2.35 to 4.43 km, with an average depth of approximately 2.73 km within the influence range of the magma chamber, which is 1.09 km shallower than the regional average. This highlights the significant impact of the magma chamber on the formation of high-temperature geothermal resources and the considerable high-temperature geothermal potential of the Changbai Mountain region.

(3) Based on the three-dimensional numerical simulation results, the geothermal resource potential of the Changbai Mountain region was calculated using integral methods, and the geothermal power generation potential of the reservoir was further estimated. The geothermal resource potential of the region is approximately 5.79 $\times$ 10^{20} J, with the magma chamber contributing an additional potential of 2.25 $\times$ 10^{19} J. The geothermal power generation potential of the region is approximately 6759.4 MWe, with the magma chamber contributing an additional potential of 262.4 MWe. These results indicate that the Changbai Mountain region possesses immense potential for geothermal power generation.

Formatting of funding sources

This study was supported by the National Key Research and Development Program of China (Grant Nos. 2021YFA0716003 and 2021YFB1507405) and Science Foundation of China University of Petroleum, Beijing (No. 2462024YJRC027).

CRediT authorship contribution statement

Jialin Song: Writing – review & editing, Writing – original draft, Visualization, Validation, Methodology, Formal analysis, Data curation. **Nansheng Qiu:** Writing – review & editing, Supervision, Resources, Project administration, Methodology, Investigation, Funding acquisition, Conceptualization. **Qianqian Feng:** Writing – review & editing, Funding acquisition. **Chuanqing Zhu:** Software, Methodology. **Yonghui Huang:** Funding acquisition. **Keyan Liao:** Writing – review & editing, Data curation. **Zhanwen Zhang:** Data curation. **Yike Zhou:** Data curation.

Declaration of competing interest

The authors declared that they have no conflicts of interest to this work. We declare that we do not have any commercial or associative interest that represents a conflict of interest in connection with the work submitted.

Data availability

Data will be made available on request.

References

Andreeva, O., Yarmolyuk, V., Andreeva, I., Borisovskiy, S., 2018. Magmatic evolution of Changbaishan Tianchi Volcano, China–North Korea: evidence from mineral-hosted melt and fluid inclusions. Petrology 26 (5), 515–545.

Chen, C., 2015. Study on the Reserve Regularity and Hydrochemical Characteristics of Geothermal Resources in Changbai Mountain Basalt Region. Jilin university.

Chen, S., Lee, S., Simutė, S., et al., 2021. Geochemical and seismic tomography constraints of two-layer magma chambers beneath the bimodal volcanism: a case study of late cenozoic volcanic rocks from ulleung island and mt. Changbai (paektu). Chem. Geol. 581, 120386.

Cheng, C., Liu, R., Wu, H., et al., 2024. Geothermal resource potential from intraplate magmatic–volcanic activities: a case study of mt. Changbai in northeast china. Geothermics. 122, 103053.

Chiodini, G., Liccioli, C., Vaselli, O., et al., 2014. The domuyo volcanic system: an enormous geothermal resource in argentine patagonia. J. Volcanol. Geotherm. Res. 274, 71–77.

Choi, S., Oh, C., Götze, H., 2013. Three-dimensional density modeling of the egm2008 gravity field over the mount paekdu volcanic area. JGR Solid Earth 118 (7), 3820–3836.

Chou, G., Fang, H., Zhong, Q., et al., 2014. Study for MT 3D Inversion in the middle and lower reaches of the Yangtze river important mineralization zones and its adjacent area. Progress in Geophysics 29 (06), 2730–2737.

Duan, M., Niu, Y., Sun, P., et al., 2022. A simple and robust method for calculating temperatures of granitoid magmas. Mineral. Petrol. 116 (1), 93–103.

Fan, X., Chen, Q., Ai, Y., et al., 2021. Quaternary sodic and potassic intraplate volcanism in northeast china controlled by the underlying heterogeneous lithospheric structures. Geology. 49 (10), 1260–1264.

Fan, X., Chen, Q., Guo, Z., 2020. High-resolution Rayleigh -wave phase velocity structure beneath the Changbaishan volcanic field associated with its magmatic system. Acta Petrologica Sinca. 36 (07), 2081–2091.

Fan, W., Guo, F., Wang, Y., et al., 2003. Late mesozoic calc-alkaline volcanism of post-orogenic extension in the northern da hinggan mountains, northeastern china. J. Volcanol. Geotherm. Res. 121 (1-2), 115–135.

Fuchs, S., 2018. The variability of rock thermal properties in sedimentary basins and the impact on temperature modelling – a danish example. Geothermics. 76, 1–14.

Gao, L., Shang, G Z G, Wei, H Q, et al., 2006. Recent geochemical changes of hot-spring cases from Tianchi volcano area,Changbai mountains,Northeast China. Seismology And Geology (03), 358–366.

Gorczyk, W., Vogt, K., 2018. Intrusion of magmatic bodies into the continental crust: 3-d numerical models. Tectonics. 37 (3), 705–723.

Guan, Y., Cui, S., Yang, G., et al., 2020. Changbaishan tianchi volcano crustal magma chambers modeling with gravity profile. Acta Petrol. Sin. 36 (12), 3840–3852.

Guo, W., Liu, J., Xu, W., et al., 2015. Reassessment of the magma system beneath Tianchi volcano,Changbaishan:Phase equilibria. Chin. Sci. Bull. 60 (35), 3489–3500.
Guo, L., Zhang, Y., Ma, S., 1996. Research on "Magma Chamber"of Changbai Mountain Volcanoes by Means of Seismic Tomography. CT Theory and Applications (01), 47–52.
Horn, S., Schmincke, H.U, 2000. Volatile emission during the eruption of Baitoushan Volcano (China/North Korea) ca. 969 AD. Bull. Volcanol. 61, 537–555.
Hakozaki, M., Miyake, F., Nakamura, T., Kimura, K., Masuda, K., Okuno, M., 2018. Verification of the annual dating of the 10th Century Baitoushan Volcano eruption based on an AD 774-775 radiocarbon spike. Radiocarbon. 60 (1), 261–268.
Jiang, D., 2021. Inversion of Gravity and Magnetic Data and Geothermal Genesis in Changbai Mountain Volcanic Area. Jilin University.
Jiang, G., 2017. Heat Flow Measurements and Lithospheric Thermal Structure in Northeastern China. University of Chinese Academy of Sciences.
Jiang, G., Hu, S., Cui, T., et al., 2023. Thermal structure beneath changbaishan volcano, northeastern asia; New insights from temperature logging and numerical modelling. Geophys. J. Int. 235 (2), 1228–1239.
Karingithi, C., Arnórsson, S., Grönvold, K., 2010. Processes controlling aquifer fluid compositions in the olkaria geothermal system, kenya. J. Volcanol. Geotherm. Res. 196 (1–2), 57–76.
Li, B., 2018. Study on the evaluation of geothermal resources in Changbai Mountain basalt area. Jilin University.
Li, C., Zhang, X., Zhang, Y., et al., 2006. Analysis of tectonic setting of changbaishan tianchi volcano. Seismological and Geomagnetic Observation and Research 27 (5), 43–49.
Li, H., 2015. Application of CSAMT to geothermal exploration in Songjianghe area. Jilin University.
Li, H., Liu, C., Tian, Y., et al., 2022. Seismic tomography of the crustal structure in northeast china. Journal of Jilin University (Earth Science Edition) 52 (1), 270–280.
Li, X., 2023. Study on Present Geothermal Field in the Northern part of the Central Depression of Songliao Basin. China University of Petroleum.
Liu, D., Fan, Y., Zhang, Y., et al., 2020. Mechanism of the Volcanic Unrest of the Changbaishan Tianchi Volcano from 2002 to 2005. Earthquake Research In China 36 (03), 561–570.
Liu, Q., Chen, S., Guo, W., et al., 2015. Research advances in the mt.changbai volcano. Bulletin of Mineralogy, Petrology and Geochemistry (4), 710–723.
Merriman, J D, Whittington, A G, Hofmeister, A M, et al., 2013. Thermal transport properties of major archean rock types to high temperature and implications for cratonic geotherms. Precambrian. Res. 233, 358–372.
Miao, S., Li, H., Chen, G., 2014. Temperature dependence of thermal diffusivity, specific heat capacity, and thermal conductivity for several types of rocks. J. Therm. Anal. Calorim. 115 (2), 1057–1063.
Ming, Y., Su, W., Fang, L., 2006. A preliminary study of types of volcanic earthquakes and volcanic activity in changbaishan, tianchi volcano. Earthquake Research in China 22 (1), 56–63.
Nanayama, F., Satake, K., Furukawa, R., Shimokawa, K., Atwater, B.F., Shigeno, K., Yamaki, S., 2003. Unusually large earthquakes inferred from tsunami deposits along the Kuril trench. Nature 424, 660–663.
Okuda, Y., Ohta, K., Hasegawa, A., et al., 2020. Thermal conductivity of fe-bearing post-perovskite in the earth's lowermost mantle. Earth. Planet. Sci. Lett. 547, 116466.
Pan, B., de Silva, S., Xu, J., et al., 2020. Late pleistocene to present day eruptive history of the changbaishan-tianchi volcano, china/dprk: new field, geochronological and chemical constraints. J. Volcanol. Geotherm. Res. 399, 106870.
Pang, Z., Huang, S., Hu, S., et al., 2014. Progress and Prospects of Geothermal Research in China (1995~2014). Chin. J. Geol. 49 (03), 719–727.
Qiu, N., 2002. Characters of thermal conductivity and radiogenic heat production rate in basins of northwest china. Chin. J. Geol. 37 (2), 196–206.
Ruan, S., Tang, J., Dong, Z., et al., 2020. Electric structrue model of tianchi volcano in changbai mountains based on three-dimensional ar-qn magnetotelluric inversion. Seismology and Geology 42 (6), 1282–1300.
Sarmiento, Z., Sagala, B., Siagian, H., 2019. The sokoria geothermal system, flores island, indonesia. Geothermics 82, 282–295.
Shakirov, A., Chekhonin, E., Popov, Y., et al., 2021. Rock thermal properties from well-logging data accounting for thermal anisotropy. Geothermics. 92, 102059.
Shi, Y., Zhang, J., 2004. The deep geodynamic background of Cenozoic volcanoes formed by intracontinental backarc expansion away from the ocean trench in northeast China. Acta Seismol. Sin. 1–8.
Stefánsson, A., 2017. Gas chemistry of icelandic thermal fluids. J. Volcanol. Geotherm. Res. 346, 81–94.
Stelling, P., Shevenell, L., Hinz, N., et al., 2016. Geothermal systems in volcanic arcs: volcanic characteristics and surface manifestations as indicators of geothermal potential and favorability worldwide. J. Volcanol. Geotherm. Res. 324, 57–72.
Sun, Q., Zhang, W., Zhu, Y., et al., 2019. Effect of high temperatures on the thermal properties of granite. Rock. Mech. Rock. Eng. 52 (8), 2691–2699.
Tang, B., Qiu, N., Zhu, C., et al., 2024. Thermal conductivity column of rocks and distribution characteristics of paleo-geothermal field in the songliao basin. Coal Geology & Exploration 52 (1), 26–35.
Tang, J., Deng, Q., Zhao, G., et al., 2001. Electric conductivity and magma chamber at the Tianchi volcano area in Changbaishan mountain. Seismology and Geology (02), 191–200.
Tiskatine, R., Bougdour, N., Idoum, A., et al., 2023. Experimental investigation on rock thermal properties under the influence of temperature. Thermochim. Acta 720, 179424.
Traineau, H., Westercamp, D., Benderitter, Y., et al., 1989. Case study of a volcanic geothermal system, Mount Pelée, Martinique. Journal of Volcanology and Geothermal Research 38 (1-2), 49–66.
Wang, F., Zhang, X., Yang, Z., 2002. 2-d crustal structure of changbaishan-tianchi volcanic region determined by seismic traveltime inversion. Acta Seismologica Sinica 24 (2), 144–152.
Wang, G., Zhang, W., Liang, J., et al., 2017. Evaluation of geothermal resources potential in china. Acta Geoscientia Sinica 38 (4), 448–459.
Wang, G., Liu, F., Lin, W., et al., 2023. The crustal heat production rate and crustal and mantle heat flow distribution in the land areas of china. Chinese Journal of Geophysics 66 (12), 5041–5056.
Wang, H., 2023. Study on formation and evolution of groundwater in Changbai Mountain area under the influence of seasonal freeze-thaw. Jilin university.
Wang, J., 2015. Geothermal and its Application. Science Press, Beijing.
Wei, F., Xu, J., Shangguan, Z., et al., 2016. Helium and carbon isotopes in the hot springs of changbaishan volcano, northeastern china; A material connection between changbaishan volcano and the west pacific plate? J. Volcanol. Geotherm. Res. 327, 398–406.
Wei, H., Liu, G., Gill, J., 2013. Review of eruptive activity at tianchi volcano, changbaishan, northeast china; Implications for possible future eruptions. Bull. Volcanol. 75 (4), 1–14.
Wei, H., Wang, Y., Jin, J., et al., 2007. Timescale and evolution of the intracontinental tianchi volcanic shield and ignimbrite-forming eruption, changbaishan, northeast china. Lithos. 96 (1-2), 315–324.
Williams, C., Reed, M., Mariner, R., 2008. A Review of Methods Applied by the U.S. Geological Survey in the Assessment of Identified Geothermal Resource. US Department of Interior, US Geological Survey.
Wu, F., Sun, D., Li, H., et al., 2002. A-type granites in northeastern china; Age and geochemical constraints on their petrogenesis. Chem. Geol. 187 (1-2), 143–173.
Wu, J., Ming, Y., Zhang, H., et al., 2007. Earthquake swarm activity in Changbaishan Tianchi volcano. Chinese Journal of Geophysics (in Chinese) 1089–1096.
Xia, B., Thybo, H., Artemieva, I M, 2020. Lithosphere mantle density of the north china craton. Jgr Solid Earth 125 (9).
Xiang, P., Xu, H., Ji, H., et al., 2022. Thermal property of granite in deep strata and its effect on thermal zone of surrounding rock. Shock Vib. 2022, 1–9.
Xu, J., Liu, G., Wu, J., et al., 2012. Recent unrest of changbaishan volcano, northeast china: a precursor of a future eruption? Geophys. Res. Lett. 39 (16).
Yan, D., Tian, Y., Zhao, D., et al., 2023. Seismicity and magmatic system of the changbaishan intraplate volcano in east asia. Journal of Geophysical Research. Solid Earth. 128 (9).
Yang, Z., Zhang, X., Zhao, J., et al., 2005. Tomographic imaging of 3-d crustal structure beneath changbaishan-tianchi volcano region. Chin. J. Geophys. 48 (1), 107–115.
Yi, J., Wang, P., Shan, X., et al., 2021. Modeling the multi-level plumbing system of the changbaishan caldera from geochemical, mineralogical, sr-nd isotopic and integrated geophysical data. Geosci. Front. 12 (5), 101171.
Yan, B., 2016. Study on the Formation Mechanism of Geothermal Water Resources in Changbai Mountain basalt area. Jilin University.
Zhang, D., Wei, J., Fu, L., et al., 2015. Formation of the jurassic changboshan-xieniqishan highly fractionated i-type granites, northeastern china: implication for the partial melting of juvenile crust induced by asthenospheric mantle upwelling. Geol. J. 50 (2), 122–138.
Zhang, J., Fan, Y., Chu, W., et al., 2024. Changbaishan Tianchi volcano geothermal system: Magma chamber and hidden high-temperature geothermal resources. Acta Seismol. Sin. 46 (4), 557–577.
Zhang, M., Guo, Z., Liu, J., et al., 2018. The intraplate changbaishan volcanic field (china/north korea): a review on eruptive history, magma genesis, geodynamic significance, recent dynamics and potential hazards. Earth-Sci. Rev. 187, 19–52.
Zhang, J., Huang, S., Fu, R., Tang, X., 2017. Application of magnetotellurics in geothermal exploration and research in volcano areas. Acta Petrologica Sinica 33 (1), 279–290.
Zhang, M., Guo, Z., Liu, J., et al., 2018. The intraplate changbaishan volcanic field (china/north korea): a review on eruptive history, magma genesis, geodynamic significance, recent dynamics and potential hazards. Earth-Sci. Rev. 187, 19–52.
Zhao, D., Lei, J., Tang, R., 2004. Origin of the Changbai intraplate volcanism in Northeast China: evidence from seismic tomography. Chin. Sci. Bull. 49 (13).
Zhang, X., Zhang, C., Zhao, J., et al., 2002. Deep seismic sounding investigation into the deep structure of the megma system in Changbaishan Tianchi Volconic Region. Acta Seismol. Sin. 24 (2), 135–143.
Zhao, R., 2019. The mechanism and genetic model of vapor-liquid circulation processes in Changbai mountain two-phase geothermal system. Jilin University.
Zhou, B., Pan, B., Yin, C., et al., 2022. New understanding of the magma evolution of changbaishan-tianchi volcano based on melts simulation. Seismology and Geology 44 (4), 831–844.
Zhu, H., Tian, Y., Zhao, D., et al., 2019. Seismic structure of the Changbai intraplate volcano in NE China from joint inversion of ambient noise and receiver functions. J. Geophys. Res.: Solid Earth 124 (5).
Zuo, Y., Sun, Y., Zhang, L., et al., 2024. Geothermal resource evaluation in the sichuan basin and suggestions for the development and utilization of abandoned oil gas wells. Renew. Energy 225, 120362.